Molecular Crystals and Liquid Crystals

ISSN: 1542-1406 (Print) 1563-5287 (Online) Journal homepage: http://www.tandfonline.com/loi/gmcl20

Synthesis, Growth and Characterization of Benzophenone-4-methoxybenzoylhydrazone Single Crystals

V. Meenatchi, K. Muthu, R. Agilandeshwari & SP. Meenakshisundaram

To cite this article: V. Meenatchi, K. Muthu, R. Agilandeshwari & SP. Meenakshisundaram (2015) Synthesis, Growth and Characterization of Benzophenone-4-methoxybenzoylhydrazone Single Crystals, Molecular Crystals and Liquid Crystals, 609:1, 205-217, DOI: 10.1080/15421406.2014.954339

To link to this article: http://dx.doi.org/10.1080/15421406.2014.954339

Mol. Cryst. Liq. Cryst., Vol. 609: pp. 205–217, 2015

ISSN: 1542-1406 print/1563-5287 online
DOI: 10.1080/15421406.2014.954339

Synthesis, Growth and Characterization of Benzophenone-4-methoxybenzoylhydrazone Single Crystals

V. MEENATCHI, K. MUTHU, R. AGILANDESHWARI, AND SP. MEENAKSHISUNDARAM*

Department of Chemistry, Annamalai University, Annamalainagar, Tamilnadu, India

Structural analysis of single crystals of benzophenone-4-methoxybenzoylhydrazone, grown by conventional slow evaporation solution growth technique from ethanol at room temperature, belong to monoclinic system with the space group $P2_1/c$ and the cell parameters are, a = *8.8380(4) Å,* b = *10.0767(4) Å,* c = *19.8146(9) Å and* V = *1736.88(13) Å^3. The functional groups present in the molecule are confirmed by FT-IR and FT-Raman spectral analyses. The ^{1}H and ^{13}C signals are confirmed by nuclear magnetic resonance spectroscopy. The powder X-ray diffraction study reveals the crystallinity of the as-grown crystal and it is compared with that of the simulated one. Mass spectrometry provides information pertaining to the structure and molecular weight of the compound. Good transmittance in the visible region is observed and the band gap energy is estimated using diffuse reflectance data by the application of Kubelka–Munk algorithm. Thermal analysis reveals the purity of the crystal. The scanning electron microscopy (SEM) studies reveal the surface morphology of the as-grown crystal. Theoretical calculations were performed using density functional theory (DFT) employing B3LYP functional and 6-31G*(d,p) *level as the basis set for to derive the optimized geometry, dipole moment, Mulliken charge population, HOMO–LUMO energies and first-order molecular hyperpolarizality (β) values. The optimized geometry closely resembles the ORTEP.*

Keywords Crystal structure; single crystal XRD; TG/DTA; NMR; band gap energy; theoretical studies

1. Introduction

Hydrazones and their metal compounds are of current interest for their physico-chemical properties and applications in many important chemical processes that include sensors, non-linear optics, medicine and others [1–6]. They possess antimicrobial [7, 8], anti-tubercular [9], anti-convulsant [10], and anti-inflammatory activities [11–13]. Moreover, some hydrazone analogues have been investigated as potential oral iron chelating drugs for the

*Address correspondence to SP. Meenakshisundaram, Department of Chemistry, Annamalai University, Annamalainagar, Tamilnadu, India. E-mail: meenakshisundaram.sp.294@annamalaiuniversity.ac.in, aumats2009@gmail.com.

Color versions of one or more of the figures in the article can be found online at www.tandfonline.com/gmcl.

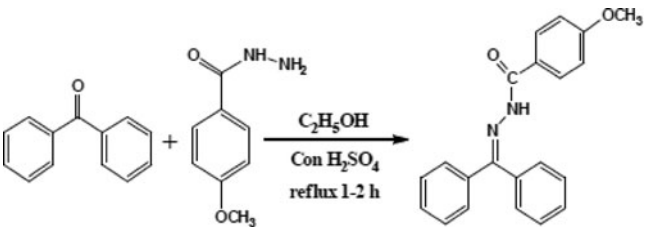

Scheme 1. Synthesis route of BPMBH.

treatment of genetic disorders such as thalassemia [14, 15] and have also been suggested as possible metal chelating agents for treating neurodegenerative disorders such as Alzheimer disease [16, 17]. The bactericidal, herbicidal, insecticidal and fungicidal properties of hydrazones are well known [18–23]. In addition, hydrazones have been found to possess analytical applications [24–27]. Recently, we have reported the synthesis, growth, structure and theoretical studies of 4-benzoylpyridine isonicotinyl hydrazone monohydrate [28], (E)-N′-(Diphenylmethylene)isonicotinohydrazide dihydrate [29] and benzophenone-2-furoyl hydrazone single crystals [30]. In the present study, we report the synthesis, growth, structure, dipole moment, hyperpolarizability and characterization of benzophenone-4-methoxybenzoylhydrazone.

2. Experimental Procedure

2.1. Synthesis and Crystal Growth

Benzophenone-4-methoxybenzohydrazide was synthesized by mixing stoichiometric amounts of benzophenone and 4-methoxybenzoydrazide in the molar ratio of 1:1. The reactants were dissolved in ethanolic medium with catalytic amount of concentrated sulphuric acid and refluxed for 1–2 hours to form aryl acid hydrazone (Scheme 1). The completion of the reaction was confirmed by thin layer chromatography. The reaction mixture was then poured in ice cold water and the precipitate obtained was filtered and dried. Purity of the compound was improved by recrystallization process using ethanol as a solvent.

Single crystals of BPMBH were grown using slow evaporation solution growth technique at room temperature. A saturated solution of BPMBH in ethanol was prepared and the solution was stirred for 3–4 hours at room temperature to obtain a homogenous solution. A beaker containing BPMBH solution was tightly covered with a thin polythene sheet to control the evaporation rate of the solvent and kept undisturbed in a dust free environment. Numerous tiny crystals were formed at the bottom of the container and the transparent colorless crystals were harvested after 20 days. Photo images of as-grown crystals are shown in Fig. 1.

3. Characterization Studies

The structural analysis of BPMBH was carried out for a selected needle of approximately $0.35 \times 0.30 \times 0.30$ mm^3 using a BRUKER AXS (Kappa APEXII) X-ray diffractometer. The powder XRD analysis was performed using a Philips X′pert Pro Triple axis X-ray diffractometer using a wavelength of 1.540 Å. FT-IR and FT-Raman spectra were recorded

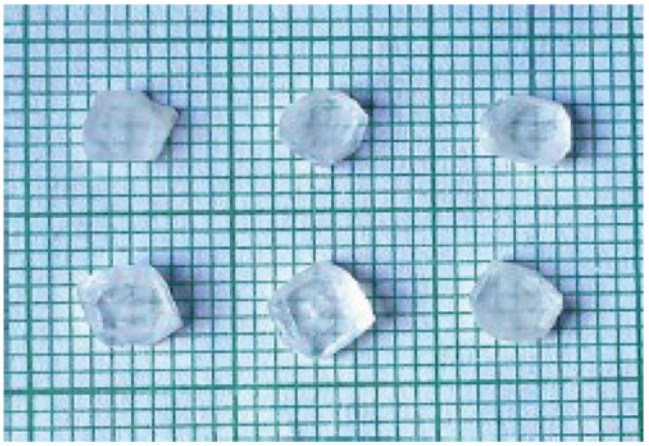

Figure 1. Photo images of as−grown BPMBH crystals.

by an NICOLET IS5 FT-IR (using the KBr pellet) and BRUKER RFS 100/S Instruments. A CARY−5E UV–vis spectrophotometer was used for the UV–vis studies. The surface morphology was observed using a JEOL JSM 5610 scanning electron microscope (SEM) with a resolution of 3.0 nm and accelerating voltage 15 kV. Thermogravimetry and differential thermal analyses were recorded on NETZSCH STA 449F3 thermal analyzer in nitrogen atmosphere. ^{1}H NMR and ^{13}C NMR spectra were recorded on BRUKER AVIII 400 MHz NMR spectrometer operating at 400.13 MHz for ^{1}H and 100.61 MHz for ^{13}C using standard parameters. BPMBH is dissolved in 0.5 ml of $CDCl_3$ solvent and TMS (tetramethylsilane) was used as an internal standard. Mass spectra were recorded on a VARIAN−SATURN 2000 GC–MS/MS spectrometer using electron impact technique. Samples were prepared by dissolving about 1 mg of compound in 5 ml of spectral grade methanol. Theoretical calculations were performed using the *GAUSSIAN 09W* [31] program package on a personal computer without any constraints on the geometry using DFT method with 6−31G(*d,p*) as the basis set [32]. By the use of the *GAUSSVIEW* 5.0 molecular visualization program [33] the optimized structure of the molecule has been visualized.

4. Results and Discussion

4.1. FT-IR and FT-Raman

In order to confirm the functional groups present in the BPMBH molecule, FT-IR spectrum was recorded (Fig. 2(a)) in the spectral range of 650–4000 cm^{-1}. The absorption band at 3365 cm^{-1} and 3318 cm^{-1} are due to N−H asymmetric and symmetric stretching vibration. The observed FT-IR and FT-Raman (Fig. 2(b)) bands of BPMBH and the assignments of vibrations are listed in Table 1.

4.2. Optical Studies

The optical reflection spectrum shows minimum absorption in the visible region and cut-off wavelength is ∼395 nm. The direct and indirect band gap energies can be obtained

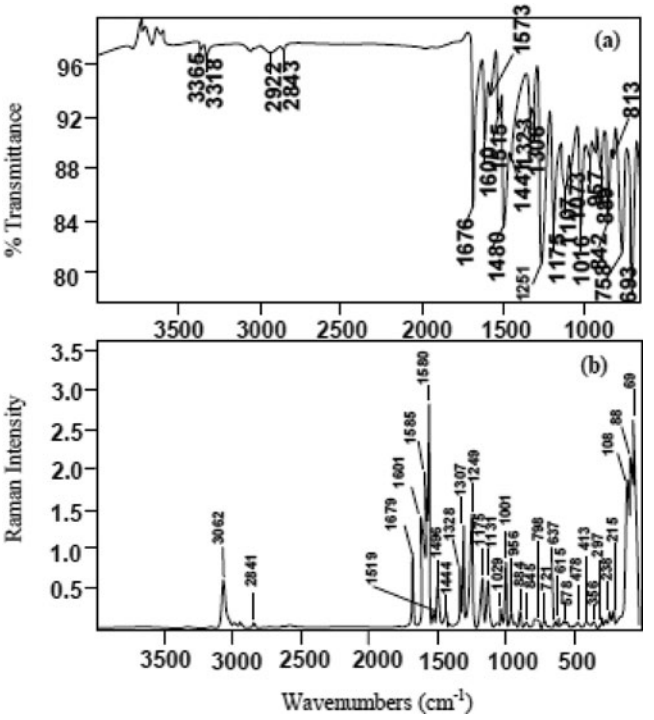

Figure 2. (a) FT−IR and (b) FT−Raman spectra of BPMBH.

from the intercept of the resulting straight lines with the energy axis at $[F(R)hv]^2 = 0$ and $[F(R)hv]^{1/2} = 0$ respectively where $F(R)$ is Kubelka-Munk function. The band gap energies of the specimen are deduced as 3.45 (direct) and 3.25 eV (indirect) as shown in Fig. 3. Using the Kubelka-Munk theory [34] providing correlation between reflectance and concentration.

Table 1. Observed vibrational bands of BPMBH (cm^{-1}).

FT-IR	FT-Raman	Assignments of vibration
1676	1679	C = O stretching
1600	1601	C = N stretching
1515,1480	1519,1496	Aromatic C = C stretching
3064	3062	Aromatic C−H stretching
1573	1580	N-H bending
1016	1029	O = C−N stretching
1175	1175	C−O−C stretching
889	884	N−N stretching
2843	2841	Aliphatic C−H stretching
842	845	Aliphatic C−H deformation
758	750	Aromatic C−H out of plane bending

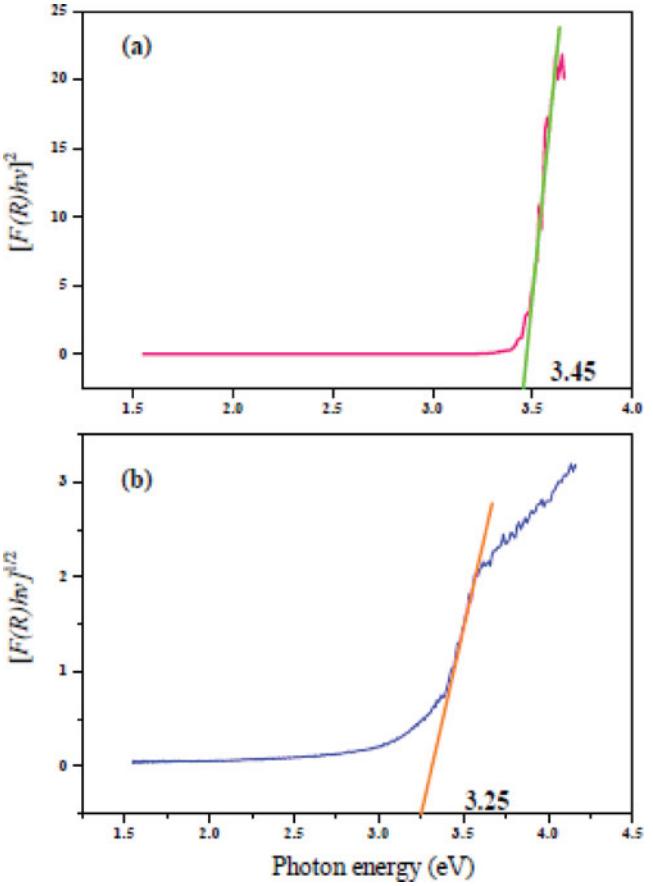

Figure 3. Tauc plots of (a) direct and (b) indirect band gap energies of BPMBH.

4.3. SEM Analysis

SEM study gives information about the external morphology and the SEM pictures of BPMBH crystals at different magnifications are given in Fig. 4. Lamellar crystals with obtuse corners are observed in the surface. Surface imperfection and crystal voids are observed.

4.4. Powder X-ray Diffraction Analysis

As-grown BPMBH crystal was finely powdered and subjected to powder XRD analysis at room temperature and all observed reflections are indexed. The indexed powder XRD patterns of the as-grown BPMBH crystal is shown in Fig. 5. The well defined Bragg's peaks at specific 2θ angles show high crystallinity of the material. Most of the peak positions in powder and simulated XRD pattern from single crystal XRD coincide and the relative intensities differ, due to preferred orientations of the sample used for diffractogram measurement. Also it could be due to the differences in the mosaic spread of powder and single crystal patterns.

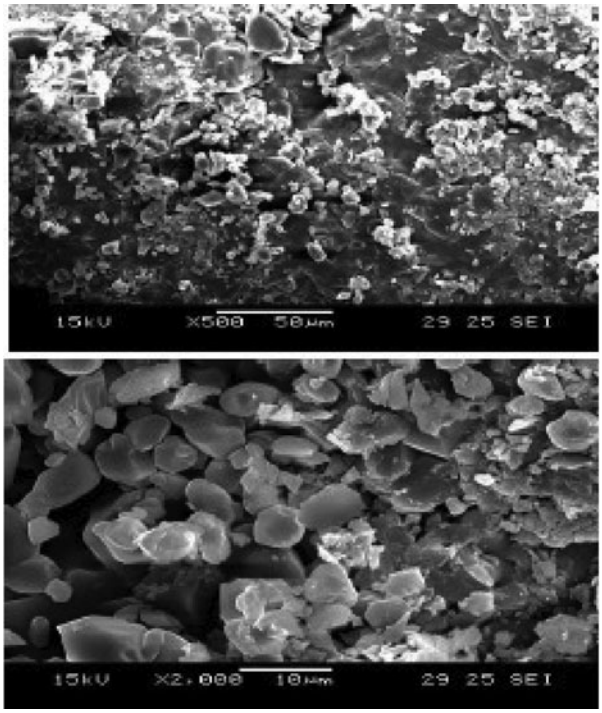

Figure 4. SEM images of BPMBH.

4.5. Thermal Analysis

TG/DTA was performed to investigate the thermal behavior of the as-grown crystals (Fig. 6). In the DTA analysis, a sharp endothermic peak at ∼175°C was assigned to the melting point, at which no weight loss has been noticed in the TG analysis. Below this endotherm,

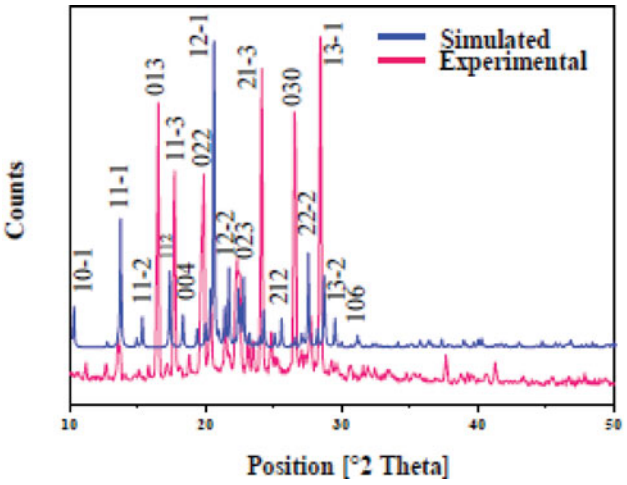

Figure 5. Powder XRD patterns of BPMBH.

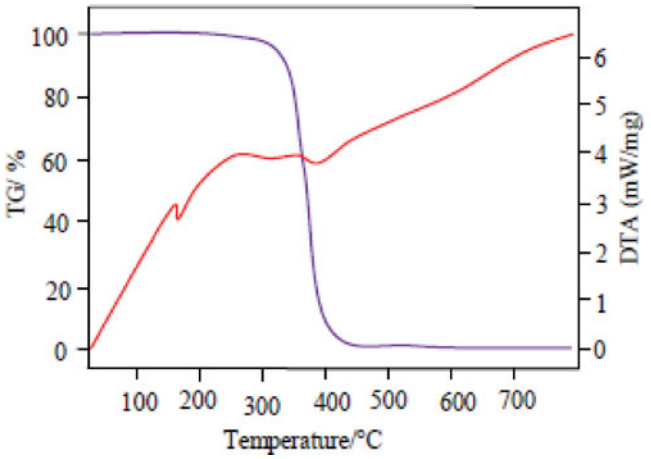

Figure 6. TG−DTA curves of BPMBH.

no exothermic peak is observed. In the thermogravimetric analysis, the material exhibits single−stage weight loss starting at ∼350°C, which may be due to decomposition of the BPMBH, and below this temperature no significant weight loss is observed. The sharpness of the endothermic peak observed with DTA curve shows the good degree of crystallinity of the material. No decomposition up to the melting point ensures the stability of the material for laser applications where the crystals are required to withstand high temperatures. The sharp endotherm is indicative of a solid-state transition for relatively pure material. The melting point was also determined using Sigma instrument melting point apparatus (∼171–173°C). The endothermic peak observed at ∼410°C is due to the decomposition of the material.

4.6. NMR and GC-Mass Spectral Analyses

^{1}H NMR spectrum of BPMBH is shown in Fig. 7. The signal at 9.02 ppm corresponds to NH proton of the amide group and the multiplet appeared in the range 7.26–7.62 ppm corresponding to ten protons, due to benzylidene protons of the phenyl group. The singlet at 6.88 ppm, corresponding to two protons, is due to the ortho protons of the methoxy phenyl ring. The signals at 8.10 and 7.69 ppm are due to the meta protons of the methoxy phenyl ring. There is a sharp singlet at 3.83 ppm, corresponding to three protons, are due to the methoxy proton of the phenyl ring.

^{13}C NMR spectrum of BPMBH is shown in Fig. 8. The signal at 162.7 ppm is due to the carbonyl carbon. The weak signal at 153.9 ppm is due to C = N group. The signal at 136.8 ppm is due to ipso carbon of the phenyl group. The benzylidene aromatic carbon appeared in the range of 128.0−130.1 ppm. The signals at 81.8 ppm and 113.9 ppm are due to ortho and meta carbons of the methoxy phenyl ring. The signal at 55.5 ppm is due to methoxy carbon of the phenyl group.

The GC−Mass spectrum of the BPMBH is shown in Fig. S1 (see supplementary information). The molecular ion peak observed at $m/z = 331$ $[(M+1)^+]$ is in good agreement with calculated value $m/z = 330$ $[M^+]$.

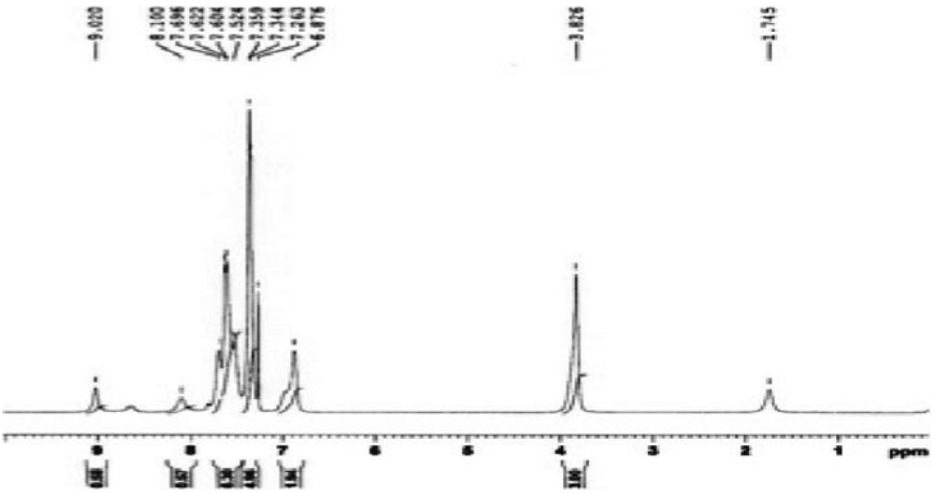

Figure 7. ^{1}H NMR spectrum of BPMBH.

4.7. Single Crystal XRD Analysis

BPMBH crystal belongs to monoclinic system with the space group $P2_1/c$ and the cell parameters are, $a = 8.8380(4)$ Å, $b = 10.0767(4)$ Å, $c = 19.8146(9)$ Å, $\alpha = \gamma = 90^{\circ}$, $\beta = 100.178(3)^{\circ}$, $V = 1736.88(13)$ Å^3 and $Z = 4$. The ORTEP is shown as Fig. 9. The crystal data and structure refinement of BPMBH listed in Table 2.

The O1 atom and the hydrazinic N2 atom are cis with respect to C8-N1 bond. The structure of the compound reveals the quasi coplanarity of the whole molecular skeleton with localization of the double bonds in the central –C = N−N−C=O which has an E-configuration with respect to the double bond of the hydrazone bridge. A trans configuration is fixed around the N2-N1 single bond of length 1.3705(17) Å. The angle O1-C8-N1

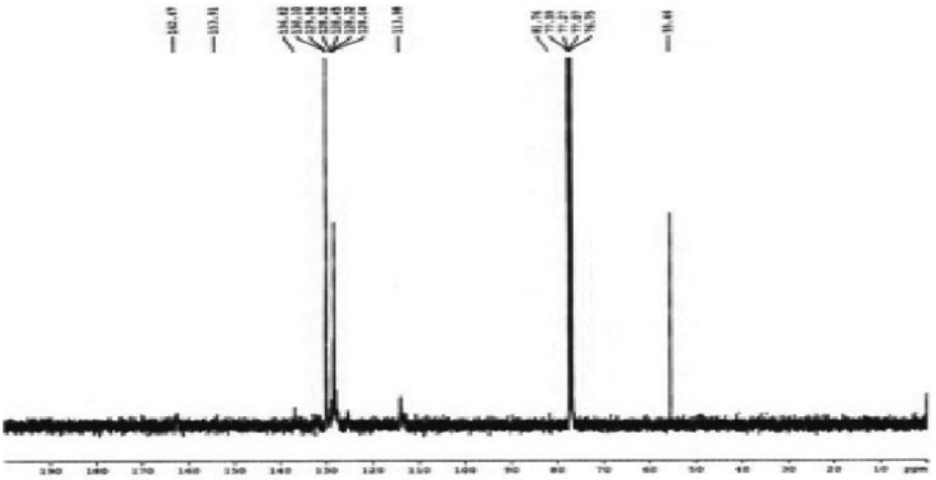

Figure 8. ^{13}C NMR spectrum of BPMBH.

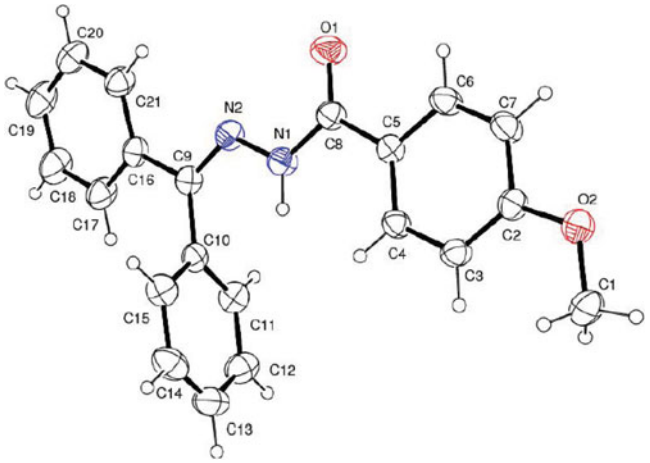

Figure 9. ORTEP diagram of BPMBH.

Table 2. Crystal data and structure refinement for BPMBH

Empirical formula	$C_{21}H_{18}N_2O_2$
Formula weight	330.37
Temperature	293(2) K
Wavelength	0.71073Å
Crystal system, space group	Monoclinic, $P2_1/c$
Unit cell dimensions	$a = 8.8380(4)$ Å, $\alpha = 90^\circ$
	$b = 10.0767(4)$ Å, $\beta = 100.178(3)^\circ$
	$c = 19.8146(9)$ Å, $\gamma = 90^\circ$
Volume	1736.88(13) Å^3
Z, Calculated density	4, 1.263 mg/m^3
Absorption coefficient	0.082 mm^{-1}
F(000)	696
Crystal size	0.35 mm × 0.30 mm × 0.30 mm
Theta range for data collection	2.09 to 25.00°
Limiting indices	$-10 \leq h \leq 9$, $-11 \leq k \leq 11$, $-23 \leq l \leq 23$
Reflections collected/unique	15318/3005 [R(int) = 0.0321]
Completeness to theta = 25.00	100%
Absorption correction	Semi-empirical from equivalents
Max. and min. transmission	0.9935 and 0.9693
Refinement method	Full-matrix least-squares on F^2
Data/restraints/parameters	3055 / 1 / 232
Goodness-of-fit on F^2	1.046
Final R indices [I > 2sigma(I)]	R1 = 0.0365, wR2 = 0.0991
R indices (all data)	R1 = 0.0535, wR2 = 0.1152
Extinction coefficient	0.023 (2)
Largest diff. peak and hole	0.144 and −0.118 e. Å^{-3}

Table 3. The calculated β components, β_{tot} value (in esu), α_{tot} value (in esu) and HOMO–LUMO (eV) for BPMBH

Components	BPMBH
β_{xxx}	839.707
β_{xxy}	−482.340
β_{xyy}	−123.784
β_{yyy}	145.928
β_{xxz}	−29.331
β_{xyz}	−33.335
β_{yyz}	−28.734
β_{xzz}	−24.203
β_{yxx}	61.1767
β_{zzz}	21.615
β_{tot} ($\times 10^{-30}$)	6.439
α_{tot} ($\times 10^{-24}$)	38.37
μ	6.6586
E_{HOMO}	−5.7217
E_{LUMO}	−1.3623
E_{HOMO}-E_{LUMO}	4.3954
E (kcal/mol)	29143.852

(121.75(14)°) is greater than O2—C5—C4 (121.82 (14)°) possibly in order to relive repulsion between lone pair of electrons on the atoms N2 and O1. The central part of the molecule C9-N2-N1-C8-O1, adopts a completely extended conformation. The bond lengths C9—N2 (1.2847 (19) Å) and C8—O1 (1.2127 (17) Å) are typical of double bonds. Molecules are linked through intermolecular O–H hydrogen bonds involving methoxy group and carbonyl group in phenyl ring. The crystal cohesion is achieved by intermolecular hydrogen bonds.

4.8. Theoretical Studies

The calculated polarizability (α), first-order molecular hyperpolarizability *(β)* and dipole moment (μ) of the specimen are 38.37 $\times$ 10^{-24} esu, 6.439 $\times$ 10^{-30} esu and 6.6586 D, respectively (Table 3). The beta value is considerably high compared to urea as standard, a required property for an NLO material. The maximum β is due to the behavior of nonzero μ values. The optimized molecular structure of BPMBH (Fig. 10) closely resembles the displacement ellipsoid diagram (Fig. 9). High β is associated with high charge transfer.

Fig. S2 (see supplementary information) shows the highest occupied molecular orbital (HOMO) and lowest unoccupied molecular orbital (LUMO) diagram of BPMBH. The frontier orbital gap facilitates in characterizing the chemical reactivity and kinetic stability of the molecule. The red and green color indicates the positive and negative values of the wave function. The HOMO is the orbital that primarily acts as an electron donor and the LUMO is the orbital that mainly acts as an electron acceptor.

The atomic charge distributions of the various atoms present in the BPMBH (Fig. 11) obtained by Mulliken population analysis [35] and the corresponding Mulliken's plot is shown as Fig. S3 (see supplementary information). From the listed atomic charge value, the oxygen (O17 and O43), nitrogen (N15 and N16), hydrogen (H18) and carbon (C4—C8,

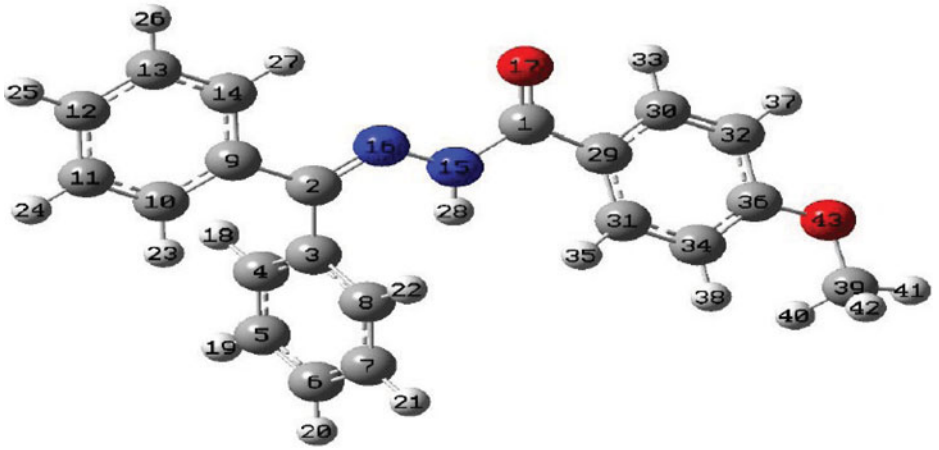

Figure 10. Optimized molecular structure of BPMBH.

C10—C14 and C30—C39) in BPMBH had a large negative charge and behaved as electron donors. The remaining atoms exhibit positive charge, which is an acceptor atom. The negative charges on nitrogen/oxygen, which is a donor atom and net positive charge on hydrogen atom, which is an acceptor atom, suggests the presence of, intermolecular hydrogen bonding interactions in BPMBH. Hydrogen bonding interaction clearly shown by the Packing diagram using single crystal XRD data (Fig. 12).

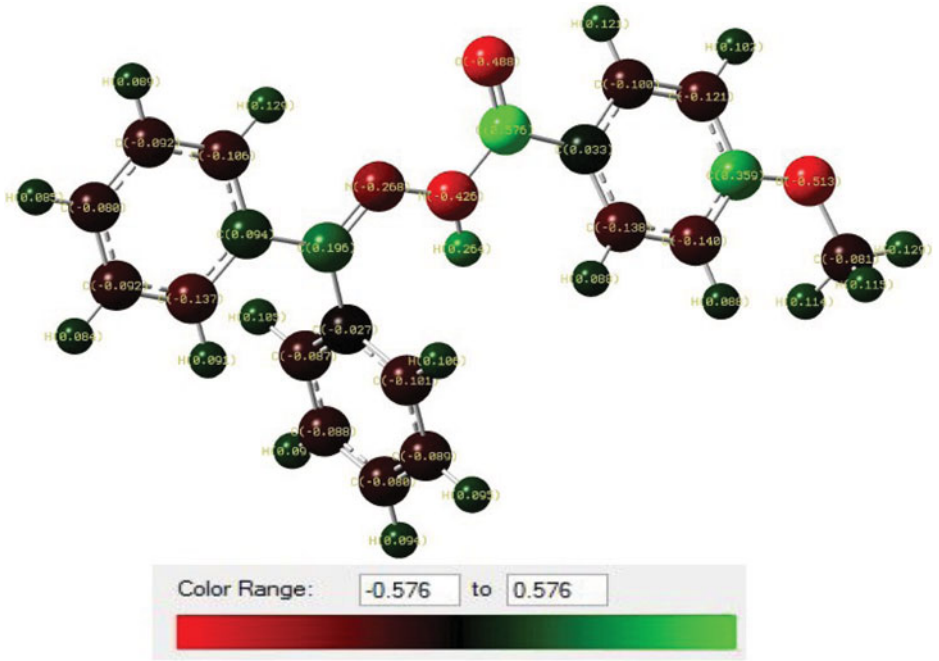

Figure 11. Mulliken atomic charge distribution for BPMBH.

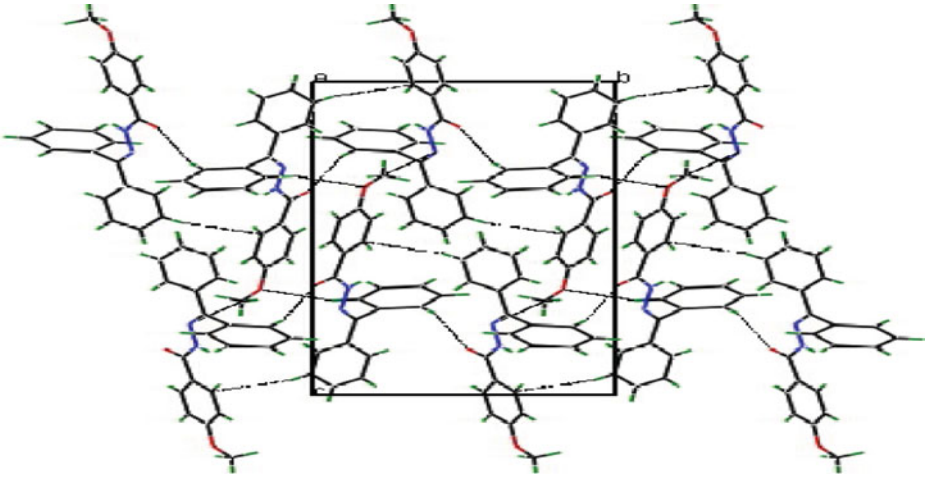

Figure 12. Packing diagram of BPMBH.

5. Conclusions

Single crystals of benzopenone-4-methoxybenzoylhydrazone were grown from an ethanolic solution by slow evaporation solution growth technique at room temperature. The product formation was confirmed single crystal X-ray diffraction analysis. FT-IR and FT-Raman spectra reveal the modes vibrations present in the molecule. The powder X-ray diffraction experimental and simulated patterns coincide with each other with varied intensity patterns. Benzopenone-4-methoxybenzoylhydrazone crystal has a wide transparency range and the band gap energies are estimated as 3.45 (direct) and 3.25 eV (indirect), using the reflectance data. The ^{1}H and ^{13}C signals of the grown crystal are identified by the NMR analyses. The TG–DTA studies reveal that the crystal is stable up to the melting point. Mass of the grown crystal is confirmed by high resolution mass spectral analysis. SEM analysis shows surface imperfection and crystal voids. The HOMO and LUMO energies clearly reveal the charge density localizations. The Mulliken charges of the molecule were also calculated and interpreted. Molecular level nonlinearity with a high first-order molecular hyperpolarizability is observed.

Acknowledgment

The authors thank SAIF, IIT Madras, Chennai for providing single crystal XRD facility.

Funding

The authors thank the Council of Scientific and Industrial Research (CSIR), New Delhi, for financial support through research grant No. 03 (1233)/12/EMR−II, and VM is grateful to CSIR project for the award of Senior Research Fellowship (SRF). KM is thankful to CSIR [9/3(0009)2K11-EMR-I], New Delhi, for the award of SRF.

Supplementary Material

CCDC 991737 contains the supplementary crystallographic data for this paper. These data can be obtained free of charge from The Cambridge Crystallographic Data Centre via.

Supplemental data for this article can be accessed at www.ccdc.cam.ac.uk/datarequest/cif.

References

[1] Armstrong, C. M., Bernhardt, P. V., Chin, P., & Richardson, D. R. (2003). *Eur. J. Inorg. Chem.*, *2003*, 1145–1156.
[2] Schmitt, J. L., Stadler, A. M., Kyritsakas, N., & Lehn, J. M. (2003). *Helvetica Chim. Acta.*, *86*, 1598–1624.
[3] Mezzina, E., Spinelli, D., Lamartina, L., Buscemi, S., Frenna, V., & Macaluso, G. (2002) *Eur. J. Org. Chem.*, *2002*, 203–208.
[4] Hegab, M. I., Hassan, N. A., El-Telbani, E. M., Farag, I. S. A., & Abdel-Megeid, F. M. E. (2003). *Heteroatom Chem.*, *14*, 223–228.
[5] Hayden, L. M., Kim, W. K., Chafin, A. P., & Lindsay, G. A. (2001). *J. Polym. Sci. Part B: Polym. Phys.*, *39*, 895–900.
[6] Pelagatti, P. *et al.* (2002) *Eur. J. Inorg. Chem.*, *2002*, 439–446 .
[7] Vinuelas-Zahinos, E., Maldonado-Rogado, M. A., Luna-Giles, F., & Barros-Garc, F. J. (2008). *Polyhedron*, *27*, 879–886.
[8] Vicini, P., Zani, F., Cozzini, P., & Doytchinova, I. (2002). *Eur. J. Med. Chem.*, *37*, 553–564.
[9] Kocyigit-Kaymakcioglu, B., & S. Rollas, (2002). *II Farmaco*, *57*, 595–599.
[10] Ragavendran, J. V. *et al.* (2007). *Eur. J. Med. Chem.*, *42*, 146–151.
[11] Bezerra-Netto, H. J. C., Lacerda, D. I., Miranda, A. L. P., Alves, H. M., Barreiro, E. J., & Fraga C. A. M. (2006). *Bioorg. Med. Chem.*, *4*, 7924–7935.
[12] Rollas, S., & Kuçukguzel, S. G. (2007). *Molecules*, *12*, 1910–1939.
[13] Ainscough, E. W., Brodie, A. M., Dobbs, A. J., Ranford, J. D., & Waters, J. M. (1998). *Inorg. Chim. Acta.*, *267*, 27–38.
[14] Ranford, J. D., Vittal, J. J., & Wang, Y. M., (1998). *Inorg. Chem.*, *37*, 1226–1231.
[15] Buss, J. L., Greene, B. T., Turner, J., Torti, F. M., & Torti, S. V. (2004). *Curr. Top. Med. Chem.*, *4*, 1623–1635.
[16] Whitnall, M., & Richardson, R. (2006). *Sem. Ped. Neurol.*, *13*, 186–197.
[17] Donnelly, P. S. *et al.* (2008). *J. Biol. Chem.*, *283*, 4568–4577.
[18] Hoyer, W., & Howath, G. A., (1973). *Chem. Abstr.*, *78*, 1608H.
[19] Dilworth, J. R. (1976). *Coord. Chem. Rev.*, *21*, 29.
[20] Alcock, J. P., Baker, H. J., & Diamautis, A. A. (1972). *Aust. J. Chem.*, *25*, 289.
[21] Sahni, S. K., Gupta, S. P., Sangal, S. K., & Rana, V. B. (1977). *J. Inorg. Nucl. Chem.*, *39*, 1098–1100.
[22] Foye, W. O., & Duvall, R. N. (1958). *J. Am. Pharm. Assoc. Sci. Ed. 47*, 285–288.
[23] Sing, N. K., Aggarwal, R. C., & Aggarwal, N. (1984). *Indian J. Chem.*, *23A*, 1011–1015.
[24] Katyal, M., & Dutty, (1975). *Talanta*, *22*, 151–166.
[25] Heit, M. L., & Ryan, D. E. (1966). *Anal. Chim. Acta*, *34*, 407–411.
[26] Jensen, R. E., & Pflaum, R. T. (1967). *Anal. Chim. Acta*, *37*, 397–400.
[27] Dey, K., Ray, S. B., Bhattacharya, P. K., Gangopadhyay, A., Bhasin, K. K., & Verma, R. D. (1985). *J. Indian Chem. Sot.*, *62*, 809–814.
[28] Meenatchi, V., Muthu, K., Rajasekar, M., & Meenakshisundaram, SP. (2014). *Spectrochim. Acta Part A.*, *124*, 423–428.
[29] Meenatchi, V., Muthu, K., Rajasekar, M., Bhagavannarayana, G., & Meenakshisundaram, SP. (2014). *Optik*, *125*, 4181–4185.
[30] Meenatchi, V., Muthu, K., Rajasekar, M., & Meenakshisundaram, SP. (2014). *Optik*, *125*, 4196–4200.
[31] Frisch, M. J., Trucks, G. W., *et al.* (2004). *Gaussion03*. Gaussian Inc., Wallingford, CT, USA.
[32] Schlegel, B. (1982). *J. Comput. Chem.*, *3*, 214–218.
[33] Frisch, A., Nielson, A. B., & Holder, A. J., (2000). *GAUSSVIEW User Manual*, Gaussian Inc., Pittsburgh, PA.
[34] Kubelka, P., & Munk, F. (1931). *Z. Tech. Phys.*, *12*, 593–601.
[35] Mulliken, R. S. (1955). *J. Chem. Phys.*, *23*, 1833–1840.